PHYSICAL REVIEW B **88**, 134201 (2013)

Solute drag by vacancies in body-centered cubic alloys

Thomas Garnier,[1,2,*] Maylise Nastar,[1] Pascal Bellon,[2] and Dallas R. Trinkle[2]
[1]*CEA, DEN, Service de Recherches de Métallurgie Physique, F-91191 Gif-sur-Yvette, France*
[2]*Department of Materials Science and Engineering, University of Illinois, Urbana-Champaign, Urbana, Illinois 61801, USA*
(Received 15 May 2013; revised manuscript received 10 July 2013; published 2 October 2013)

Transport coefficients, the elements of the so-called Onsager matrix, are essential quantities for modeling solid-state kinetics controlled by diffusion. Focusing on diffusion in binary alloys with a body-centered cubic crystal structure, we investigate the drag of solute atoms by vacancies, an effect induced by kinetic correlations. To accomplish this, an analytic method—the self-consistent mean field method—is extended to take into account interactions between the solute atom and a vacancy up to the third nearest neighbor sites. We identify kinetic effects involving one or more frequencies. Analytic results are compared with select atomic kinetic Monte Carlo simulations. We show that (1) solute drag is a more general phenomena than previously assumed, (2) it can induced by association and dissociation exchanges, and (3) we identify the mechanisms involved.

DOI: 10.1103/PhysRevB.88.134201 PACS number(s): 61.82.Bg, 66.30.Fq, 72.15.−v

I. INTRODUCTION

Atomic transport plays a ubiquitous role during the fabrication and processing of materials as a route to develop microstructures that optimize properties. In particular, atomic diffusion in crystalline alloys controls the chemical homogenization of castings,[1,2] the rate of precipitation of second phases during heat treatments,[3,4] or the buildup of solute segregation at microstructural elements such as dislocations, grain boundaries, and surfaces.[5–7] In addition, atomic transport can limit the stability of a microstructure at finite temperature. When a material is irradiated, point defects are created homogeneously in the material and migrate toward sinks like dislocations or grain boundaries. When defect fluxes are coupled to atomic fluxes, they can lead to phenomena like radiation-induced segregation, as observed in austenitic steels where chromium depletion appears at grain boundary under irradiation.[7–10] In iron-copper alloys, vacancies and copper atoms are strongly bound and vacancies drag along the copper atoms which can facilitate the copper precipitation in the vicinity of vacancy sinks.[11] Flux coupling can even lead to the nucleation of thermodynamically unstable phases like Ni_3Si in undersaturated Ni(Si) alloys under irradiation.[6,12]

In a near equilibrium system, the atomic flux J^α of a chemical species α per unit area is linearly related to the gradients of chemical potential $\nabla\mu^\beta$ of all species β by the Onsager matrix $L_{\alpha\beta}$:

$$\vec{J}^\alpha = -\sum_\beta L_{\alpha\beta}\vec{\nabla}\left(\frac{\mu^\beta}{k_B T}\right), \tag{1}$$

where k_B stands for the Boltzmann constant and T for the temperature. The Onsager matrix thus describes the flux coupling at work in radiation-induced segregation. The Onsager matrix is also required for accurate mesoscopic kinetic simulations such as the phase field approach.[13,14] However, in most cases only simplified models are used for the description of kinetic properties; e.g., DICTRA only includes the diagonal terms.[15] These approximations limit the possibilities for these models to make quantitative predictions, as they ignore effects induced by correlation terms in the Onsager matrix such as solute drag by vacancies. In particular, in the presence of a gradient of chemical potential of vacancies, solute atoms can diffuse even if the chemical potential for the solute is spatially uniform under the influence of the nonzero off-diagonal terms in the Onsager matrix that are due to kinetic correlations. This phenomenon is observed experimentally on quenched dilute alloys.[16–18] If a sufficiently stable solute-vacancy complex is formed, the vacancy will drag the solute during its displacement.[19] If the complex dissociates after only a few jumps, site conservation results in the solute atoms moving in the opposite direction of the vacancy flux.

The crystal structure plays a significant role in the onset of solute drag. Consider a dilute alloy, with a face-centered cubic (fcc) lattice. A vacancy may move around the solute from one first nearest neighbor (NN) site to another—in energetically equivalent configurations—without breaking the solute-vacancy complex as there are NN sites of the vacancy that are also NNs of the solute. If the rate for the vacancy to move from a first nearest neighbor site to another is large compared to the rate of dissociation of the solute-vacancy complex, the vacancy will stay on an orbit of first nearest neighbor sites (which we will refer to as "1" orbit) long enough to allow drag to take place. In contrast, in the body-centered cubic (bcc) lattice, first nearest neighbor sites are not mutual neighbors. Hence, a vacancy on a first nearest neighbor site of a solute atom can either exchange position with the solute or leave the first nearest neighbor sites of the solute after one jump. Finally, in a dilute binary alloy on a bcc lattice, the displacements of a vacancy can be described using four frequencies if solute-vacancy interactions are limited to first nearest neighbor sites.[20]

First-principles thermodynamics have been very successful in predicting the equilibrium structure and properties of materials and a growing effort is being made to obtain similarly kinetic properties of alloys by computing the jump frequencies.[2,4,11,21–28] Density functional theory (DFT) results can then be coupled with analytic models[22–24,27] or atomic kinetic Monte Carlo simulations[11,21,28,29] to compute the Onsager matrix. Analytic methods are extremely computationally efficient, since only a single matrix inversion is required to obtain the Onsager matrix.[30] However, analytic methods are usually limited to the four frequency model,[31] and in the most advanced case, second nearest neighbor interactions

have been only partially taken into account.[32,33] Moreover, a truncation of the kinetic correlations is required. Using one such model, it has been concluded that no drag effect should be expected when solute-vacancy interactions are limited to first nearest neighbor sites.[11,28,31] In contrast, atomic kinetic Monte Carlo (AKMC) simulations are not limited by the number of frequencies considered (cf. Ref. 30, and references therein). However, when complex atomic interactions or highly correlated kinetics are involved—as in the case of solute drag—the computational cost of AKMC simulations can make their use impractical. This limitation is important as the accuracy of the results provided by DFT calculations comes at the cost of ever more complex interatomic interactions, and for which analytic methods have not yet been developed.

The aim of this work is to understand the origin of vacancy-induced drag effect in bcc alloys. For that purpose, numerous calculations of the Onsager matrix are required for highly correlated systems. In order to overcome the limitations discussed in the previous paragraph, and in order to gain a physical insight, we rely on the self-consistent mean field (SCMF) method[34,35] to efficiently and systematically compute the Onsager matrix and we extend this method to take into account complex interactions. We calculate all the coefficients (L_{ij}) of the Onsager matrix and we identify solute drag via the ratio L_{BV}/L_{BB}, for solute B and vacancy V, similarly to Anthony.[36] This ratio is positive when the solute atoms are dragged by the vacancies, and negative otherwise. The sign is determined by L_{BV}, which measures the correlation in the displacement of solute atoms and vacancies, as L_{BB} is always positive.

We first describe the extension of the SCMF method to better take into account kinetic correlations and atomic interactions up to third nearest neighbor sites in bcc alloys and introduce a general nomenclature for vacancy-atom exchange in the dilute limit. Next, the occurrence of solute drag in bcc alloys with interactions up to the third NN sites is studied using SCMF calculations and AKMC simulations on some selected cases. The effect of each atomic frequency is studied independently in the case of an ideal solid solution, and some collective effects are explored to identify the phenomena at the origin of solute drag by the vacancy. Finally, the SCMF calculations are applied to (1) a model alloy with interactions up to the third nearest neighbor, and (2) for a Fe(Cu) alloy.

II. ANALYTIC CALCULATIONS OF THE ONSAGER MATRIX BY THE SCMF METHOD

The SCMF method was developed initially for vacancy-controlled diffusion in regular solid solutions (corresponding to a mean field Bragg-Williams approximation of alloys)[34] and later improved to take into consideration pair correlations,[35] leading to numerically exact solutions for binary dilute alloys. Calculations based on this method were, however, limited for the fcc structure to the five frequency model and kinetic correlations were considered up to the first nearest neighbor sites only (usually called first shell approximation, here denoted 1NN), or to the first nearest neighbor sites of the first nearest neighbor sites of the solute (second shell approximation, here denoted 1NN1NN).[35] These results agreed with other analytic methods.[30] In order to quantitatively describe solute drag in complex bcc alloy models, we extend the SCMF method to take into account vacancy-solute interactions up to the third nearest neighbor sites and kinetic correlations integrated up to the third nearest neighbor sites of these third nearest neighbor sites (denoted 3NN3NN) in bcc structures. First, we briefly review the SCMF approach to calculate the Onsager matrix and extend it to the case of anisotropic structures. The application to the dilute limit is then presented, and a general nomenclature of vacancy-mediated diffusion events is introduced. Some of the details required to perform the numerical computation in the 3NN3NN approximation are provided in Appendix A.

A. Self-consistent mean field formalism

1. Out-of-equilibrium formalism

An alloy can be represented by a system of interacting atoms and vacancies distributed on a rigid lattice. A state of the alloy is then defined by a vector $\mathbf{n}$, the components of which are the occupation numbers of all species on all sites $\{n_1^A, n_1^B, \ldots, n_1^v; n_2^A, n_2^B, \ldots, n_2^v; \ldots\}$ such that $n_i^X = 1$ if the site i is occupied by the species $X \in \{v, A, B \ldots\}$ and zero otherwise. Let $w_{\mathbf{n}\to\mathbf{m}}$ be the transition rate probability between two configurations $\mathbf{n}$ and $\mathbf{m}$ through a single event. We consider a system where consecutive events are considered to be independent random events mediated by a vacancy, with stationary probability.

Let $P_0(\mathbf{n})$ be the equilibrium probability to find the system in a state $\mathbf{n}$, at a temperature T. This probability can be used as a reference and the out-of-equilibrium probability $P(\mathbf{n},t)$ to find the system in the state $\mathbf{n}$ at time t can be written as

$$\hat{P}(t) = \hat{P}_0 \exp\left[(k_B T)^{-1}\left(\delta\Omega(t) + \sum_i \sum_\alpha \delta\mu_i^\alpha n_i^\alpha - \hat{h}(t)\right)\right], \tag{2}$$

where the "hat" superscript "ˆ" denotes a configuration-dependent quantity, e.g., $\hat{P}_0 \equiv P_0(\mathbf{n})$, $\delta\Omega(t)$ is the normalization constant of the out-of-equilibrium part of the probability, k_B is the Boltzmann constant, $\delta\mu_i^\alpha$ stands for the out-of-equilibrium part of the chemical potential of the chemical species α relative to vacancy on site i, and $\hat{h}$ is an effective Hamiltonian. The effective Hamiltonian $\hat{h}$ can be written as a cluster expansion,[37] limited to pairs in the case of a dilute binary alloy,

$$\hat{h}(t) = \frac{1}{2!}\sum_{\alpha,\beta,i\neq j} v_{i,j}^{\alpha,\beta}(t) n_i^\alpha n_i^\beta, \tag{3}$$

where $v_{i,j}^{\alpha,\beta}$ are two-body effective interactions. The deviation from equilibrium is captured with $\delta\mu_i^\alpha$ and $\hat{h}$. The SCMF method focuses on the calculation of the effective interactions necessary to describe a steady state solution imposed in the presence of uniform gradient of chemical potential. For the steady-states probability, SCMF finds fluxes that are proportional to the gradients of chemical potential to determine the Onsager matrix.

2. The moments equations

Under a uniform gradient of chemical potential, a steady state solution contains the correlations in the movement of

the species that leads to the Onsager matrix. Using detailed balance, we find relations between the moment equations of the master equation. For any function $\hat{A}$ of the configuration $\mathbf{n}$ we define the equilibrium and out-of-equilibrium averages: $\sum_{\{\mathbf{n}\}} A(\mathbf{n})P_0(\mathbf{n}) = \langle \hat{A} \rangle$ and $\sum_{\{\mathbf{n}\}} A(\mathbf{n})P(t,\mathbf{n}) = \langle \hat{A} \rangle^{\mathrm{oe}}$. The SCMF method is based on the master equation

$$\frac{dP(\mathbf{n})}{dt} = \sum_{\dot{\mathbf{n}}} w_{\dot{\mathbf{n}}\to\mathbf{n}} P(\dot{\mathbf{n}}) - w_{\mathbf{n}\to\dot{\mathbf{n}}} P(\mathbf{n}), \tag{4}$$

where $w_{\dot{\mathbf{n}}\to\mathbf{n}}$ is the rate of transition from configuration $\dot{\mathbf{n}}$ to configuration $\mathbf{n}$. Considering transitions involving only an exchange between a vacancy ν on a site s and an atom α on a site i, the transition can be written $w_{\dot{\mathbf{n}}\to\mathbf{n}} = \hat{w}_{is}^{\alpha\nu}$. The time derivative of the moments $\langle n_i^\alpha \rangle^{\mathrm{oe}}, \langle n_i^\alpha n_j^\beta \rangle^{\mathrm{oe}}$ of the master equation are computed. These derivatives are approximated by considering the first order term of the Taylor expansion with respect to $(k_\mathrm{B}T)^{-1}\hat{h}(t)$. Then, the time derivative of the first moment is

$$\frac{d\langle n_i^\alpha \rangle^{\mathrm{oe}}}{dt} = -\sum_s J_{i\to s}^\alpha, \tag{5}$$

where

$$k_\mathrm{B}T\, J_{i\to s}^\alpha = -\left\{\left\langle n_i^\alpha n_s^\nu \hat{w}_{is}^{\alpha\nu}\left[\left(\delta\mu_s^\alpha - \delta\mu_i^\alpha\right) - \left(\hat{h}_s^\alpha - \hat{h}_i^\alpha\right)\right]\right\rangle\right\}, \tag{6}$$

and $\hat{h}_s^\alpha$ is the derivative of the effective Hamiltonian with respect to the variable n_s^α. The elements $J_{i\to s}^\alpha$ are the the atomic fluxes of species α from site i to site s and are usually nonzero only if i is a NN of s. The second moment derivative provides another equation:

$$\begin{aligned} k_\mathrm{B}T & \frac{d\langle n_i^\alpha n_j^\beta \rangle^{\mathrm{oe}}}{dt} \\ &= \sum_{s\neq i\neq j} \left\langle n_j^\beta \left\{ n_i^\alpha n_s^\nu \hat{w}_{is}^{\alpha\nu}\left[\left(\delta\mu_s^\alpha - \delta\mu_i^\alpha\right) - \left(\hat{h}_s^\alpha - \hat{h}_i^\alpha\right)\right]\right\}\right\rangle \\ &\quad + \sum_{s\neq i\neq j} \left\langle n_i^\alpha \left\{ n_j^\beta n_s^\nu \hat{w}_{js}^{\beta\nu}\left[\left(\delta\mu_s^\beta - \delta\mu_j^\beta\right) - \left(\hat{h}_s^\beta - \hat{h}_j^\beta\right)\right]\right\}\right\rangle. \end{aligned} \tag{7}$$

In a steady state, all time derivatives are zero, and Eqs. (6) and (7) can be used to compute the effective interactions. In a dilute alloy, only pair correlations are relevant and it is unnecessary to consider higher moments as all higher moments can be written as products of first and second order moments. Finally, symmetry can be used to reduce the number of relevant variables. Considering a Bravais lattice under a uniform gradient of chemical potential along the unit vector $\vec{u}$, the chemical potential can be defined at any point X from the chemical potential at a reference point O as $\mu(X) = \mu(O) + \overrightarrow{OX}\cdot\vec{\nabla}(\frac{\mu}{k_bT})$, where $\vec{\nabla}(\frac{\mu}{k_bT}) = \|\vec{\nabla}(\frac{\mu}{k_b})\|\cdot\vec{u}$. Two pairs of sites or "bonds" ij and $i'j'$ that are identical under a point group operation of the crystal which leave $\vec{u}$ unchanged can be considered equivalent: $ij \equiv i'j'$. They are grouped in an equivalence class $\{ij\}$ and we use the notation $\overline{ij}$ for a representative member of the class. The number of relevant classes can be reduced by considering that the effective interactions are antisymmetric with respect to the bond variable $v_{\overline{ij}}^{\alpha\beta} = -v_{\overline{ji}}^{\alpha\beta}$ and the species $v_{\overline{ij}}^{\alpha\beta} = -v_{\overline{ij}}^{\beta\alpha}$. The classes of bonds normal to $\vec{u}$ cancel out, and only classes of strictly positive projection on $\vec{u}$ are required. Defining the set of relevant equivalence classes $\mathbf{E}(\vec{u})$, and $\{\overline{ij}\}$ a set of their representatives, we need to only solve for two-body effective interactions $v_{\overline{ij}}^{\alpha\beta}$; the number of unknown variables is thus reduced to one for each of these classes. In the following we use $\vec{e}_{is}$ to designate the vector linking sites i and s and for any class we choose a representative $\overline{ij}$. Using the antisymmetry of the effective interactions, we write $\gamma_{\overline{mj},ik} = \mathrm{sign}(\vec{e_{ik}}\cdot\vec{u})$ if $mj \equiv ik$ and is null otherwise.

A calculation taking into account all classes provides an exact evaluation of the Onsager matrix in the case of a dilute binary alloy. However, this infinite set has to be truncated in practice. In the 1NN approximation, a single class is kept, corresponding to the bonds between first nearest neighbor sites. In the 1NN1NN approximation, the first nearest neighbor sites of the first nearest neighbor sites are kept, leading to five distinct classes. Finally, in the 3NN3NN approximation developed for this work, the bonds linking sites up to the third nearest neighbors of third nearest neighbors are considered, for a total of 14 distinct classes.

Equation (7) can be solved. For that purpose we define the vectors $\vec{M}$ by $\vec{M}_{\overline{ij}}^{\alpha\beta,\sigma} = \vec{0}$ unless $\sigma = \alpha$ or $\sigma = \beta$ and then

$$\begin{aligned} \vec{M}_{\overline{ij}}^{\alpha\beta,\alpha} &\equiv \sum_{s\neq i\neq j} \left\langle n_j^\beta n_i^\alpha n_s^\nu \hat{w}_{is}^{\alpha\nu}\right\rangle \vec{e}_{is}, \\ \vec{M}_{\overline{ij}}^{\alpha\beta,\beta} &\equiv -\sum_{s\neq i\neq j} \left\langle n_j^\alpha n_i^\beta n_s^\nu \hat{w}_{is}^{\beta\nu}\right\rangle \vec{e}_{is}. \end{aligned} \tag{8}$$

For atomic species $\alpha,\beta,\gamma,\zeta$ and classes $\overline{ij}$ and $\overline{pq}$, we define the matrix T

$$\begin{aligned} T_{\overline{ij},\overline{pq}}^{\alpha\beta,\eta\zeta} \equiv\ & \delta_{\alpha,\eta}\sum_s \left(\sum_k \left\langle n_k^\zeta n_j^\beta n_i^\alpha n_s^\nu \hat{w}_{is}^{\alpha\nu}\gamma_{ik,\overline{pq}}\right\rangle - \sum_k \left\langle n_k^\zeta n_j^\beta n_i^\alpha n_s^\nu \hat{w}_{is}^{\alpha\nu}\gamma_{sk,\overline{pq}}\right\rangle\right) \\ & - \delta_{\beta,\zeta}\sum_s \left(\sum_k \left\langle n_k^\eta n_j^\beta n_i^\alpha n_s^\nu \hat{w}_{js}^{\beta\nu}\gamma_{jk,\overline{pq}}\right\rangle - \sum_k \left\langle n_k^\eta n_j^\beta n_i^\alpha n_s^\nu \hat{w}_{js}^{\beta\nu}\gamma_{sk,\overline{pq}}\right\rangle\right). \end{aligned} \tag{9}$$

These notations allow one to write Eq. (7) for a steady state more simply:

$$\sum_\sigma \vec{M}_{\overline{ij}}^{\alpha\beta,\sigma}\cdot\vec{\nabla}\left(\frac{\mu^\sigma}{k_BT}\right) = T_{\overline{ij},\overline{pq}}^{\alpha\beta,\eta\zeta} v_{\overline{pq}}^{\eta\zeta}. \tag{10}$$

Thus the inversion of the T matrix provides the effective interactions. To obtain the Onsager matrix, we define a bare mobility for each class represented by $\overline{is}$,

$$l_{\overline{is}}^{\alpha\beta,(0)} \equiv \delta_{\alpha\beta}\langle n_i^\alpha n_s^\nu \hat{w}_{is}^{\alpha\nu}\rangle, \tag{11}$$

where δ is the Kronecker symbol; and for each pair of classes represented by $\overline{is}$ and $\overline{mj}$,

$$\Lambda_{\overline{is},\overline{mj}}^{\alpha,\alpha\gamma} \equiv \sum_k \langle \gamma_{\overline{mj},ik} n_i^\alpha n_s^\nu n_k^\gamma \hat{w}_{is}^{\alpha\nu}\rangle. \tag{12}$$

Finally using Eqs. (11), (12), and (6) a new flux equation is obtained

$$J_{i\to s}^\alpha = -\sum_\beta l_{\overline{is},(0)}^{\alpha\beta} \vec{e}_{is}\cdot\vec{\nabla}\left(\frac{\mu^\alpha}{k_B T}\right) + 2\sum_{\overline{mj},\gamma} \Lambda_{\overline{is},\overline{mj}}^{\alpha,\alpha\gamma} \nu_{\overline{mj}}^{\alpha\gamma}. \tag{13}$$

Using Eq. (10) this equation then becomes

$$J_{i\to s}^\alpha = \sum_\beta \left(-l_{\overline{is},(0)}^{\alpha\beta}\vec{e}_{is} + 2\sum_{\overline{mj},\overline{pq},\gamma,\beta,\sigma,\zeta} \Lambda_{\overline{is},\overline{mj}}^{\alpha,\alpha\gamma}(T^{-1})_{\overline{mj},\overline{pq}}^{\alpha\gamma,\sigma\zeta}\vec{M}_{\overline{pq}}^{\sigma\zeta,\beta}\right)\cdot\vec{\nabla}\left(\frac{\mu^\beta}{k_B T}\right), \tag{14}$$

where the first term on the right-hand side is the mobility in the absence of kinetic correlations and the second is the correlation term. Thus, the total flux can be obtained by summing over all the volume $V^{\rm tot}$ of the crystal the flux through each pair i,s of sites

$$J_{\vec{u}}^\alpha = \frac{1}{2V^{\rm tot}}\sum_{is} J_{i\to s}^\alpha \vec{e}_{is}. \tag{15}$$

From this equation can be deduced the Onsager matrix

$$L_{\vec{v},\vec{u}}^{\alpha\beta} = \frac{1}{2V^{\rm tot}}\sum_{is}\left(\left[l_{\overline{is},(0)}^{\alpha\beta}\vec{e}_{is} - 2\sum_{\overline{mj},\overline{pq},\gamma,\sigma,\zeta}\Lambda_{\overline{is},\overline{mj}}^{\alpha,\alpha\gamma}(T^{-1})_{\overline{mj},\overline{pq}}^{\alpha\gamma,\sigma\zeta}\vec{M}_{\overline{pq}}^{\sigma\zeta,\beta}\right]\cdot\vec{u}\right)\vec{e}_{is}\cdot\vec{v}, \tag{16}$$

where $L_{\vec{v},\vec{u}}^{\alpha\beta}$ has the unit of atoms per second and per meter for a flux expressed as atoms per second and per area. The cubic symmetry of the bcc lattice induces an isotropy of the diffusion properties, and the Onsager matrix can be written as the scalar $L_{\alpha\beta}$.

B. Application to the dilute limit

1. General nomenclature of vacancy-mediated kinetic events

In the case of a binary dilute alloy, where we consider vacancy-mediated kinetic events only, each transition from one state to another is due to the jump of an atom from an atomic site into the vacancy. A systematic and convenient nomenclature of these events can be defined. As illustrated in Fig. 1, three specific site occupancies are involved at most during a jump in the dilute case: the jumping atom site, the vacancy site, and the site where the nearest solute atom is located. Thus, a three index naming system can be chosen, with each index defining the relationship between two of these atoms. Let a be the distance (in nearest neighbor distance) from the site of the jumping atom to the vacancy site, b the distance from the site of the jumping atom to the solute site, and c the distance from the site of the solute to the vacancy site. As a consequence, b designates the vacancy-solute distance after the jump, while c is the distance before the jump. Moreover, for any distance beyond the solute-vacancy interaction range, the value ∞ is assigned to the index, as the numerical value is no longer relevant. The type of jump is identified with an index ζ corresponding to the five frequency notation illustrated in Fig. 2: $\zeta = 2$ for a jump of the solute atom, $\zeta = 0$ for a jump of a matrix atom without any solute in the interaction area, $\zeta = 1$ for a jump between two sites interacting with the solute, $\zeta = 3$ for a dissociative jump leading outside the interaction area, and $\zeta = 4$ for an associative jump leading toward the interaction area. The transition frequency from configuration **n** to **m** can hence be written

$$w_{\mathbf{n}\to\mathbf{m}} = w_{abc}^{(\zeta)}. \tag{17}$$

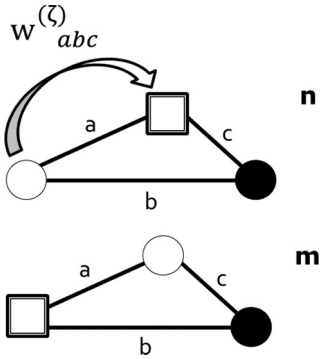

FIG. 1. Schematic of a vacancy jump in a dilute alloy in the initial configuration **n** (top) and final configuration **m** (bottom). The filled circles represent the solute atom, the open circle a matrix atom, and the squares a vacancy, while a,b,c are the distances between two species, obtained by counting the NN shells. The frequency $w_{\mathbf{n}\to\mathbf{m}}$ is $w_{abc}^{(\zeta)}$; the frequency starts from a shell c from the solute and finishes in a shell b. a indicates the jump distance and ζ the "type" of jump.

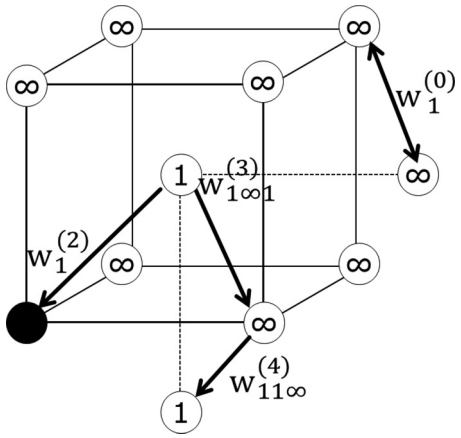

FIG. 2. Vacancy jump frequencies in a dilute bcc binary alloy with first nearest neighbor interactions. Arrows indicate the direction of the jumps for a vacancy at a site. The solute atom is represented by a filled circle, and the numbers on lattice sites indicate the distance from the solute atom site, while an ∞ indicates sites beyond the range of the interactions.

The ζ index is partly redundant with the three others: when $\zeta = 0$ or $\zeta = 2$ the indices b and c are no longer relevant and can be omitted, leading to a more compact notation. In a dilute binary bcc alloy, when jumps of the vacancy are limited to first nearest neighbor sites and solute-vacancy interactions are limited to first nearest neighbor sites, only four frequencies are necessary to describe diffusion: $w_1^{(0)}, w_1^{(2)}, w_{1\infty1}^{(3)}, w_{11\infty}^{(4)}$. The four frequency model[20,38] is thus retrieved and is illustrated in Fig. 2. Similarly, for a dilute binary bcc alloy with third nearest neighbor interactions that will be investigated in this work, all kinetic events can be described through 12 different frequencies, which are similarly represented in Fig. 3: $w_1^{(0)}, w_1^{(2)}, w_{121}^{(1)}, w_{112}^{(1)}, w_{131}^{(1)}, w_{113}^{(1)}$, $w_{1\infty1}^{(3)}, w_{1\infty2}^{(3)}, w_{1\infty3}^{(3)}, w_{11\infty}^{(4)}, w_{12\infty}^{(4)}, w_{13\infty}^{(4)}$. Note that for bcc structure, only jumps where $a = 1$ are permitted. However, this index can take different values under stress or in different structures when several jump distances exist and is kept here for that purpose.[39,40]

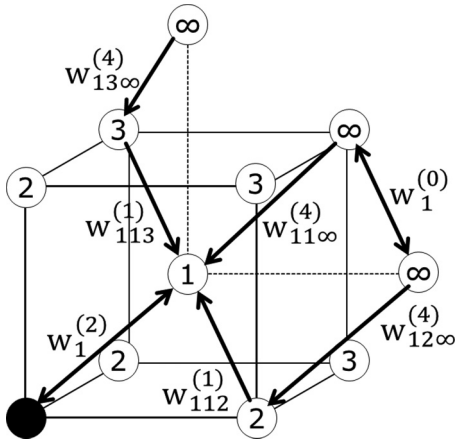

FIG. 3. Vacancy jump frequencies in a dilute bcc binary alloy with third nearest neighbor interactions. Arrows indicate the direction of the jumps for a vacancy at a site. The solute atom is represented by a filled circle, and the numbers on lattice sites indicate the distance from the solute atom site, while an ∞ indicates sites beyond the range of the interactions. Names of the return jumps have been omitted for the sake of clarity.

2. *Averages in the dilute limit*

In a dilute binary alloy $A(B)$ with a single vacancy, a single solute atom at most can be found in a finite region of space and the probability to find a configuration $\mathbf{n}$ depends only on the distance d between the vacancy and the nearest solute atom B. The probability $P_B(d)$ to find a B atom on a site at a distance d from a given vacancy is $P_B(d) = c_B e^{-(k_B T)^{-1} F(d)} = c_B y_d^{Bv}$ at the first order in c_B, where $F(d)$ is the solute vacancy binding energy at a distance d. Similarly, the probability $P_A(d)$ to find on that site a matrix atom A is $P_A(d) = 1 - c_B y_d^{Bv}$. The thermodynamic average of a quantity is obtained using this distribution probability, multiplied by the probability c_v to find a vacancy on a site.

For the sake of simplicity, we group in a single notation the three point averages $W_{abc}^{(\zeta)} = \langle n_i^\alpha n_j^\beta n_s^v w_{abc}^\zeta \rangle$, where a is the distance between sites i and s, b is the distance between sites i and j, and c is the distance between j and s, and the indices ζ, a, b, c refer to the four index systematic nomenclature defined in Sec. II B.

As in the dilute limit, w_{abc}^ζ depends only on the position of the nearest solute atom and vacancy, and it is independent from the configuration once n_i^α and n_j^β are known. Thus $W_{abc}^{(\zeta)}$ is the product of the jump frequency $w_{abc}^{(\zeta)}$ by its related thermodynamic prefactor due to the three-point average and

$$\begin{aligned} W_{abc}^{(\zeta)} &= c_v c_B y_a^{Bv} w_{abc}^{(\zeta)} \quad \text{if} \quad \zeta = 2 \\ &= c_v c_B y_c^{Bv} w_{abc}^{(\zeta)} \quad \text{otherwise.} \end{aligned} \tag{18}$$

Similarly, we group in a single notation the two point averages $\mathfrak{X}_{abc}^{(\zeta)} = \langle n_i^\alpha n_s^v w_{abc}^\zeta \rangle$. These two-point averages can be expressed as sums of three-point averages. For $\zeta \neq 0$, $\mathfrak{X}_{abc}^{(\zeta)} = \sum_{j,\beta} \langle n_i^\alpha n_j^\beta n_s^v w_{abc}^\zeta \rangle$, and results identical at the first order in c_B to the three-point averages are obtained. The case $\zeta = 0$ is specific as it corresponds to the probability *not* to have any solute atom in the neighborhood of the vacancy. Using results from Eq. (18), we obtain at the first order in c_B for $\zeta = 0$:

$$\mathfrak{X}_a^{(0)} = c_v \left(1 - c_B \left(13 + 8y_1^{Bv} + 6y_2^{Bv} + 12y_3^{Bv}\right)\right) w_{abc}^{(\zeta)},$$

while for $\zeta \neq 0$,

$$\mathfrak{X}_a^{(\zeta)} = W_{abc}^{(\zeta)} \quad \text{otherwise.} \tag{19}$$

We note that in Ref. 35 and previously in Ref. 30 the effect of the binding energies in the expression of $\mathfrak{X}_a^0$ has been missed, which corresponds to considering $y_1^{Bv} = y_2^{Bv} = y_3^{Bv} = 1$ for that specific term. However, at finite temperature, the binding energies have to be taken into account to accurately predict L_{AA}.[41]

For example of an SCMF average, in a dilute $A(B)$ binary alloy, for first NN sites i and j, if the vacancy-solute

interactions are restricted to first nearest neighbor sites,

$$\sum_s \left\langle n_s^\nu n_j^B n_i^A w_{is}^{A\nu} \right\rangle = N_{S1} W_{111}^{(1)} + N_{S4} W_{11\infty}^{(4)} = N_{S1} y_1^{BV} c_B c_\nu w_{111}^{(1)} + N_{S4} c_B c_\nu w_{11\infty}^{(4)}, \quad (20)$$

where N_{S1} is the number of first NN sites of i which are also first NN sites of j, and N_{S4} is the number of NN sites of i which are not first NN sites of j nor j itself. As a consequence, for a crystal structure with z first NN sites, $N_{S4} + N_{S1} + 1 = z$. In a bcc structure $N_{S1} = 0$ and $N_{S4} = 7$, while in a fcc structure $N_{S1} = 4$ and $N_{S4} = 7$. Detailed balance also relates the ratios of jump frequencies. For example, in the case of a bcc crystal with first nearest neighbor interactions described by the four frequency model, $y_1^{B\nu} = \frac{w_{1\infty 1}^{(4)}}{w_{11\infty}^{(3)}}$. In the dilute case, the exact Onsager matrix can then be expressed as a function of the jump frequencies and concentrations only.

III. ONSET OF DRAG EFFECT WITHIN THE FOUR FREQUENCY MODEL

The four frequency model serves as a reference for describing diffusion by vacancies in bcc alloys with solute-vacancy binding energy limited to first nearest neighbor sites. According to Refs. 28,31, and 42, no solute drag by the vacancy should happen within this model due to the absence of sites being both nearest neighbor of the solute and of one of its nearest neighbor sites. The question of solute drag in the four frequency model was investigated using SCMF calculations and assessed on select cases using AKMC simulations. For that purpose a dilute binary alloy on a bcc lattice is chosen, with an unmixing tendency. Vacancy-solute interactions are described using a broken bond model (see Appendix C) and with a vacancy-solute binding interaction E_1^b limited to first nearest neighbor sites, resulting in exchange frequencies $w^{(i)} = \nu^{(i)} e^{\beta E_i^b}$, where E_i^b is the energy in the initial configuration and $\nu^{(2)} = \nu^{(0)} = 1$, $\nu^{(3)} = \nu^{(4)}$. Simulations were performed above the critical temperature T_c, at a temperature $k_B T = 4.74 E_1^b \approx 1.5 k_B T_c$. Figure 4 presents the ratio L_{BV}/L_{BB} obtained by SCMF calculations with

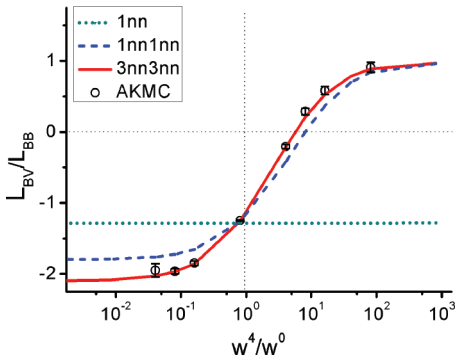

FIG. 4. (Color online) L_{BV}/L_{BB} ratio in a dilute bcc binary alloy described by the four frequency model as a function of the ratio $w^{(4)}/w^{(0)}$. Circles represent the results of AKMC simulations, while the solid (3NN3NN), dotted (1NN), and dashed (1NN1NN) lines represent SCMF calculations in the different approximations.

different kinetic approximations as a function of $w^{(4)}/w^{(0)}$. In calculations made in the 1NN approximation, no drag effect is predicted in bcc alloys: In this case, L_{BV} is always negative, in agreement with Ref. 31. However, for a large enough $w^{(4)}/w^{(0)}$ ratio, a drag effect appears according to SCMF calculations in the 1NN1NN approximation, in contradiction with the results obtained in the 1NN approximation. We note that the 1NN1NN approximation had been already developed in the past with different methods,[32,33,43] even if its results had not been applied specifically to the study of solute drag. The SCMF result in the 3NN3NN approximation confirms the results obtained in the 1NN1NN approximation.

In order to validate the SCMF results and the choice of effective interaction cutoff, atomic kinetic Monte Carlo simulations are performed to compute Onsager matrices using atomic jump frequencies identical to the ones used in SCMF calculations (see Appendix B). AKMC simulations were performed using a 2×16^3 site simulation box containing a single solute atom and a vacancy. The initial configuration is obtained by choosing random locations for the vacancy and the solute atom, and equilibrating the system for one Monte Carlo step (MCS), i.e., 2×16^3 vacancy jumps. Displacements of the atoms are recorded during 100 MCS and the values averaged over 10^5 simulations. The Onsager matrix is obtained using the Kubo-Green formula:[43]

$$L_{\alpha\beta} = \left\langle \frac{R^\alpha R^\beta}{6V\tau} \right\rangle, \quad (21)$$

where V is the atomic volume and R^α is the total displacement of all atoms of type α during the integration time τ. As can be seen in Fig. 4, the AKMC simulations confirm the SCMF predictions, as solute drag by the vacancies does appear, in quantitative agreement with the SCMF results in the 3NN3NN approximation, which predict a drag effect for $w^{(4)}/w^{(0)} > 6$. In contrast, the 1NN1NN approximation provides only a qualitatively correct prediction.

Predicting drag requires taking into account long-range correlations: It is completely missed by calculations in the 1NN approximation. The calculations in the 1NN1NN approximation, however, predict drag, which indicates that drag involves the sites surrounding the first nearest neighbor sites. As can be seen in Fig. 2, while first nearest neighbor sites are not connected by other first nearest neighbor sites on a bcc lattice, they are, however, connected by second or third nearest neighbor sites. The exchange frequencies toward and from these sites are the frequencies $w_{(4)}$ and $w_{(3)}$. If $w^{(4)}/w^{(0)}$ is large enough, the vacancy can thus turn around the solute many times, alternating between first nearest neighbor sites and more distant ones on a path that we define as the "1+" orbit. As this orbit is beyond the range considered in the 1NN approximation, that approximation misses its influence, and solute drag is not predicted. The underlying idea that the solute-vacancy pair has to remain bound is valid, but from a *kinetic* point of view, which involves not only the equilibrium position but also the saddle-point energies, and not from a thermodynamic point of view. This behavior illustrates the key mechanism behind drag, which is directly related to the ability of the vacancy to jump around the solute faster than to jump away from it.

To conclude, the example presented attests to the ability of the 3NN3NN SCMF calculations to take into account highly correlated kinetics and provide values of the Onsager matrix in quantitative agreement with AKMC simulations. This example also shows that solute drag by vacancies in dilute binary alloys on bcc lattices can happen in even the most simple systems, in particular, at low temperature where the effect of a difference between the migration enthalpies is enhanced. An accurate description of the kinetic event and a careful calculation of the kinetic properties are thus required to predict the behavior of these systems.

IV. DRAG EFFECT MECHANISM IN THE 12 FREQUENCY MODEL

The 3NN3NN approximation of the SCMF model allows us to evaluate the impact on the Onsager matrix of the 12 frequencies required to describe an alloy with solute-vacancy interactions up to the third nearest neighbor sites. However, considering the high number of frequencies, a complete parametric study with respect to all the frequencies is out of reach. Thus, to identify the main trends, the impact of each frequency on the drag effect is first evaluated independently for an ideal solid solution. In this case, the absence of solute-vacancy interactions reduces the number of free parameters to six, allowing one to more easily study the effect of each of them. Collective effects involving several frequencies are then discussed.

A. Independent effect of each frequency

The drag effect is not only determined by the vacancy-solute binding energy, but also by the ability of a vacancy to remain in the vicinity of the solute atom for a sufficient number of consecutive jumps. Such kinetic effects can be studied on an ideal solid solution, which corresponds to the high temperature limit of any alloy, and where vacancy-solute binding energy is negligible. If all frequencies were equal, no solute drag would take place. The 1NN1NN approximation in Ref. 33 provides then the ratio $L_{BV}/L_{BB} = -1.3546$, while the calculations in the 3NN3NN approximation give $L_{BV}/L_{BB} = -1.3651$, in slightly better agreement with Manning's reference calculation[45] that yields the value $L_{BV}/L_{BB} = -1.388$ for the noninteracting alloy. We study the effect of each frequency by varying one frequency while all others remain constant. As detailed balance requires $w^d_{1XY} = w^d_{1YX}$ for each XY pair, only six frequency ratios are explored so that the solute-vacancy binding energy is zero.

In Fig. 5, the ratio L_{BV}/L_{BB} is represented for an ideal solid solution with all attempt frequencies equal but one, as a function of the ratio of attempt frequencies. As the vacancy-solute exchange does not change the position of the barycenter of the vacancy-solute pair, it does not affect the L_{BV}/L_{BB} ratio. In contrast, the $w^{(1)}_{112}$ and $w^{(1)}_{113}$ frequencies allow the vacancy to move around the solute by respectively alternating between first nearest neighbor and second nearest neighbor sites, or first nearest neighbor sites and third nearest neighbor site, which we refer to as a "1-2" orbit and a "1-3" orbit, respectively. In the four frequency model, these jumps were grouped together with $w^{(4)}_{11\infty}$ in a single $w^{(4)}_{11\infty}$

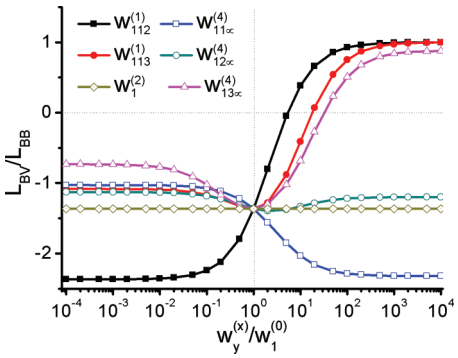

FIG. 5. (Color online) Parametric study of L_{BV}/L_{BB} in a dilute bcc binary alloy within the 12 frequency model. All drag ratios are computed using the SCMF method in the 3NN3NN approximation. For each curve, all frequencies but the designated one are equal.

frequency. The $w^{(4)}_{11\infty}$ frequency was shown to be responsible for solute drag in bcc dilute alloys with first nearest neighbor interactions on the $1+$ orbit, and similarly increasing $w^{(1)}_{112}$ and $w^{(1)}_{113}$ induces drag effect, as was the case in the four frequency model. The $w^{(4)}_{11\infty}$ has the opposite effect through its dissociative counterpart $w^{(3)}_{1\infty 1} = w^{(4)}_{11\infty}$ as it allows the escape of the vacancy from the neighborhood of the solute toward a fifth nearest neighbor site from which the vacancy cannot directly jump back to a first, second, or third nearest neighbor site, forbidding it a quick return. This reduces the drag, and indeed the ratio L_{BV}/L_{BB} increases with $w^{(4)}_{11\infty}$. These pathways of the vacancy are represented in Fig. 6.

Within the 12 frequency model, jumps that do not involve first nearest neighbor sites can also induce drag, as can be seen in Fig. 5 with the effect of the $w^{(4)}_{13\infty}$ frequency. As in the four frequency model where solute drag can be induced by successive $w^{(4)}_{11\infty}$ and $w^{(3)}_{11\infty}$ jumps, in the 12 frequency model the vacancy can turn around the solute by alternating

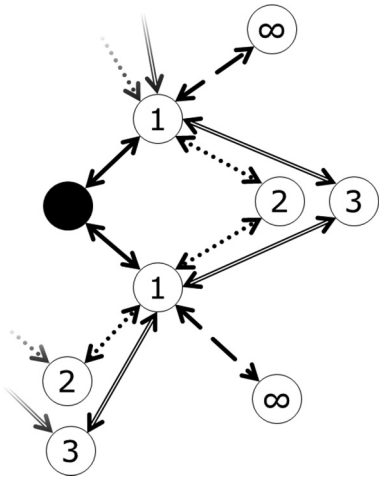

FIG. 6. Schematic pathways of the vacancy around the solute atom in a bcc alloy involving first nearest neighbor sites. The black atom represents the solute, and the arrows the possible vacancy-atom exchanges, with a different style of line for each type of bond.

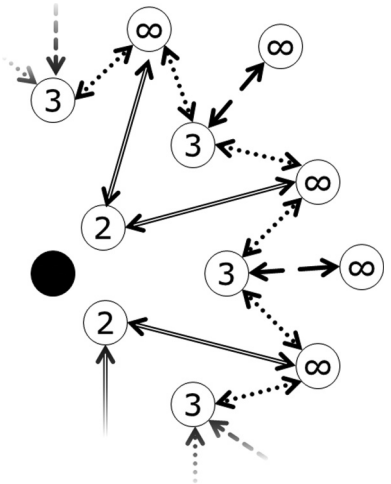

FIG. 7. In a bcc alloy, schematic pathways of the vacancy around the solute atom that do not involve first nearest neighbor sites. The black atom represents the solute, and the arrows the possible vacancy-atom exchanges, with a different style of line for each type of jump.

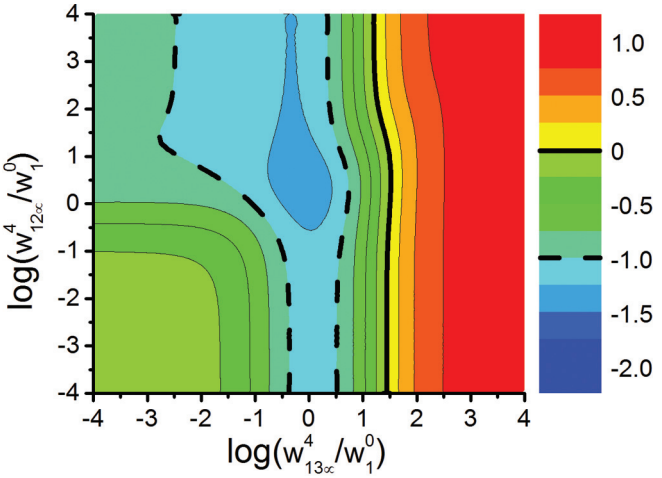

FIG. 8. (Color online) Contour map of L_{BV}/L_{BB} as a function of the $w^{(4)}_{12\infty}$ and $w^{(4)}_{13\infty}$ frequencies. The black continuous line signals the onset of solute drag.

$w^{(4)}_{13\infty}$ and $w^{(3)}_{1\infty3}$ jumps on a "3+" orbit. Finally, the $w^{(4)}_{12\infty}$ frequency which controls the jumps from second to fourth nearest neighbor sites has a limited impact; vacancies on fourth nearest neighbor sites can return to second or third nearest neighbor sites, but no orbit around the solute is possible by alternating $w^{(4)}_{12\infty}$ and $w^{(3)}_{1\infty2}$ jumps only. Figure 7 illustrates these behaviors by showing the paths of the vacancy around the solute that do not involve first nearest neighbors. A path exists that involves the $w^{(4)}_{12\infty}$ frequency, through the complex sequence of sites 2-4-3-4-, etc. This orbit is controlled by both $w^{(4)}_{12\infty}$ and $w^{(4)}_{13\infty}$, and increasing the first frequency is not sufficient for that orbit to induce solute drag according to the results in Fig. 5.

Finally, it should be noted that from case to case, drag appears for very different values of the frequency ratios: It appears for a ratio of $w^{(1)}_{112}/w^{(0)}_1 = 5$ on the 1-2 orbit, but a ratio of 20 is required on the 1-3 orbit and 30 on the "3-4" orbit. Such large ratios are unlikely to be present in real alloys solely based on the attempt frequencies, but can easily be expected at finite temperature for suitable migration enthalpies. In such cases, the solute-vacancy binding energy will have to be taken into account, and it is unlikely that only one frequency will depart from the others.

B. Collective effects

The terms of the Onsager matrix, and especially the drag ratio L_{BV}/L_{BB}, are highly nonlinear functions of the jump frequencies. Thus the kinetic behavior cannot be fully predicted on the basis of the previous analysis, as collective effects involving several jump frequencies can appear. In the previous section, it has been seen that the vacancy could turn around the solute by passing through the sequence of sites 2-4-3-4, depending on both $w^{(4)}_{12\infty}$ and $w^{(4)}_{13\infty}$. In order to study the importance of this orbit, the drag ratio L_{BV}/L_{BB} has been computed as a function of these frequencies (while all others were taken equal to 1) using the SCMF method in the 3NN3NN approximation. The result is shown in Fig. 8. It can be seen that for $w^{(4)}_{13\infty}/w^{(0)}_1 \geqslant 30$ solute drag takes place, without the $w^{(4)}_{13\infty}/w^{(0)}_1 \geqslant 30$ frequency having much influence. This seems to indicate that the threshold for the 2-4-3-4 orbit to allow solute drag is the same or higher than for the 3-4 orbit. No qualitatively new collective behavior appears in this case.

Surprisingly, as shown in Fig. 8, the $w^{(4)}_{12\infty}$ frequency seems to have a greater influence for low $w^{(4)}_{13\infty}$. This behavior has been further investigated by computing the drag ratio in the $(w^{(4)}_{11\infty}, w^{(4)}_{13\infty})$ plane for different values of the $w^{(4)}_{12\infty}$ frequency. In Fig. 9 these results are shown for $w^{(4)}_{12\infty}/w^{(0)}_1 \in [1/10, 10]$. For $w^{(4)}_{13\infty} \geqslant 30$, a drag effect is reported for any values as could be expected from the single frequency study. However, a less trivial behavior appears as solute drag takes place when the three associative frequencies are *low enough simultaneously*, while in all other cases solute drag appears when incoming frequencies become *large enough*. This phenomenon occurs for moderate values of the frequencies such as $w^{(4)}_{11\infty} = w^{(4)}_{12\infty} = w^{(4)}_{13\infty} = 0.1w^{(0)}_1$, which makes it more likely to be of practical significance. As these three frequencies control the escape rate of the vacancy, simultaneously reducing the three of them results in isolating from the matrix a volume corresponding to the solute and its first, second, and third nearest neighbors. The crystal can then be divided into three different volumes, a trap that corresponds to these first, second, and third nearest neighbor sites, a transition shell, and the bulk. When all jumps in the transition shell are significantly slower than the jumps both in the bulk and within the trap, the vacancy is kinetically trapped: If a vacancy goes inside the trap, many jumps will take place before the vacancy escapes. The vacancy will thus be able to drag the solute before escaping. In this case, and to the opposite of the other mechanisms described in this work, solute drag appears even if the jump frequencies within the trap are lower than the frequencies in the bulk, as long as they remain considerably higher than the frequencies in the transition area.

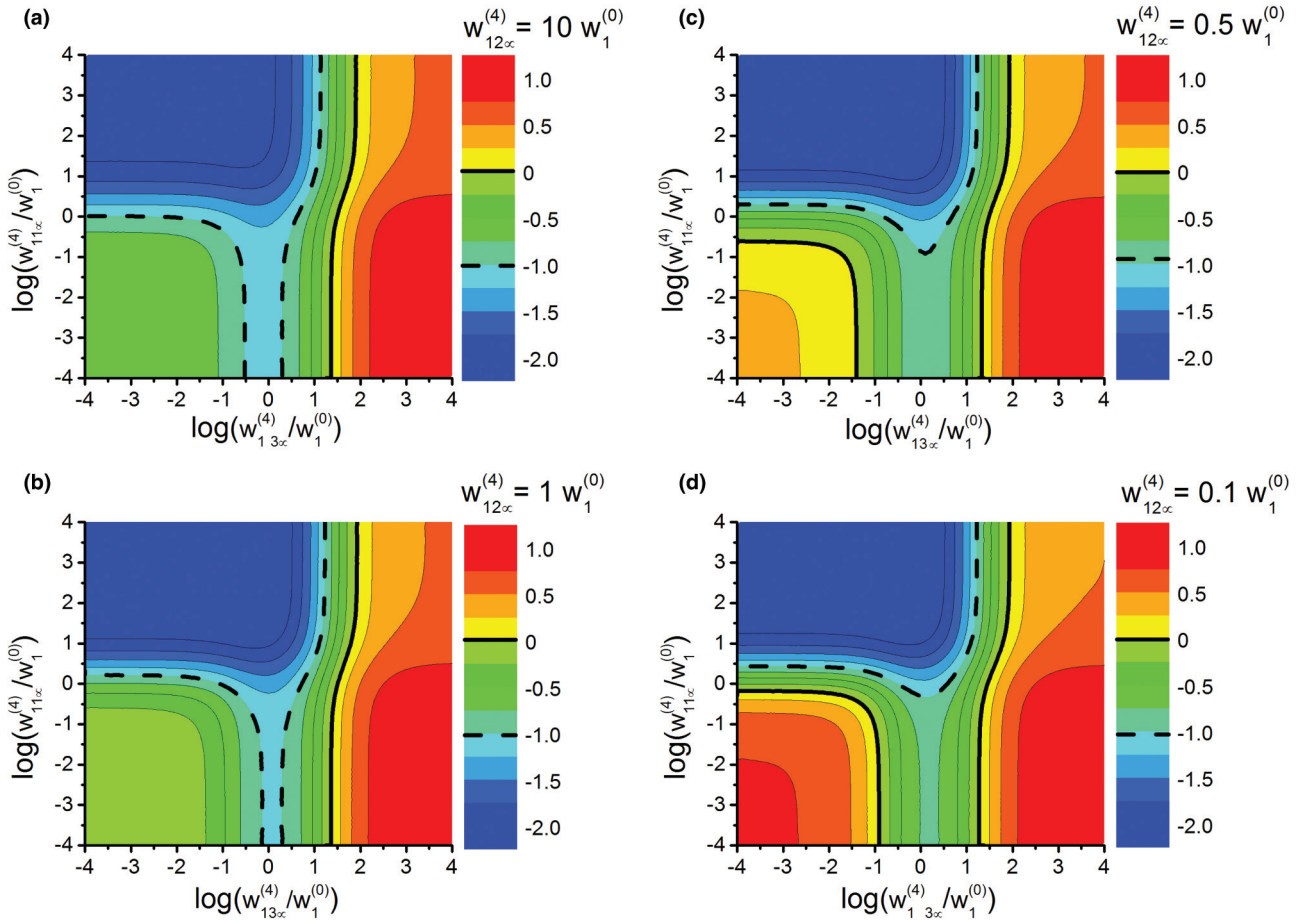

FIG. 9. (Color online) Contour map of the L_{BV}/L_{BB} ratio as a function of the $w^{(4)}_{13\infty}$ and $w^{(4)}_{11\infty}$ frequencies. (a) for $w^{(4)}_{12\infty} = 10w_0$, (b) for $w^{(4)}_{12\infty} = w_0$, (c) for $w^{(4)}_{12\infty} = 0.5w_0$, and (d) for $w^{(4)}_{12\infty} = 0.1w_0$. The black continuous line signals the onset of solute drag. The dashed line, used for clarity, corresponds to $L_{BV} = -L_{BB}$.

V. DRAG EFFECT IN ALLOYS WITH FIRST, SECOND, AND THIRD NEAREST NEIGHBOR INTERACTIONS

The calculations for the ideal solid solution provide a good basis to interpret the different effects leading to drag. However, solute-vacancy binding energy usually cannot be neglected. It leads to a splitting of frequencies that were identical in the ideal solid solution case, like $w^{(1)}_{112}$ and $w^{(1)}_{121}$. This does not affect, however, the number of variables, as these split frequencies remain related through detailed balance. During the transition from an initial configuration i toward a final configuration f, the migration enthalpy that controls the transition rate can be written as

$$E_{\text{mig}} = E^S_{i,f} - E_i, \tag{22}$$

where E_i is the energy in the initial configuration and $E^S_{i,f}$ is the saddle-point energy of the transition. Different models exist to describe this migration energy. Using the 3NN3NN approximation, a parametric study of two different models for the migration energy are presented, first with an alloy obeying the kinetically resolved activation barrier (KRA) approximation, and later in the case of an alloy where frequencies are described by the broken bond model. The case of a real alloy, the Fe(Cu) alloy, is finally treated.

A. Kinetically resolved activation barrier approximation

In the KRA approximation, used for example under different names by Senhaji *et al.*[46] and later by Van der Ven *et al.*[47] or Vincent *et al.*,[48] the migration barriers are approximated by considering them as linearly dependent on the energy of the initial and final states. In a dilute bcc or a fcc alloy the migration barrier is defined as

$$E^S_{i,f} = E^0 + \tfrac{1}{2}\left(E^b_f + E^b_i\right), \tag{23}$$

where E^b_f and E^b_i are the binding energies in the final and initial configurations and E^0 is the migration barrier for a jump at infinite distance from any solute atom. As a consequence, the saddle-point energy and thus the migration energy depend on both the initial and final configuration energies, but not on other parameters, and the frequencies automatically obey detailed balance. With interactions up to the third nearest neighbor sites, the kinetic behavior of an alloy thus depends only upon the three binding energies between the solute and a vacancy on a first, second, or third nearest neighbor site, that we will

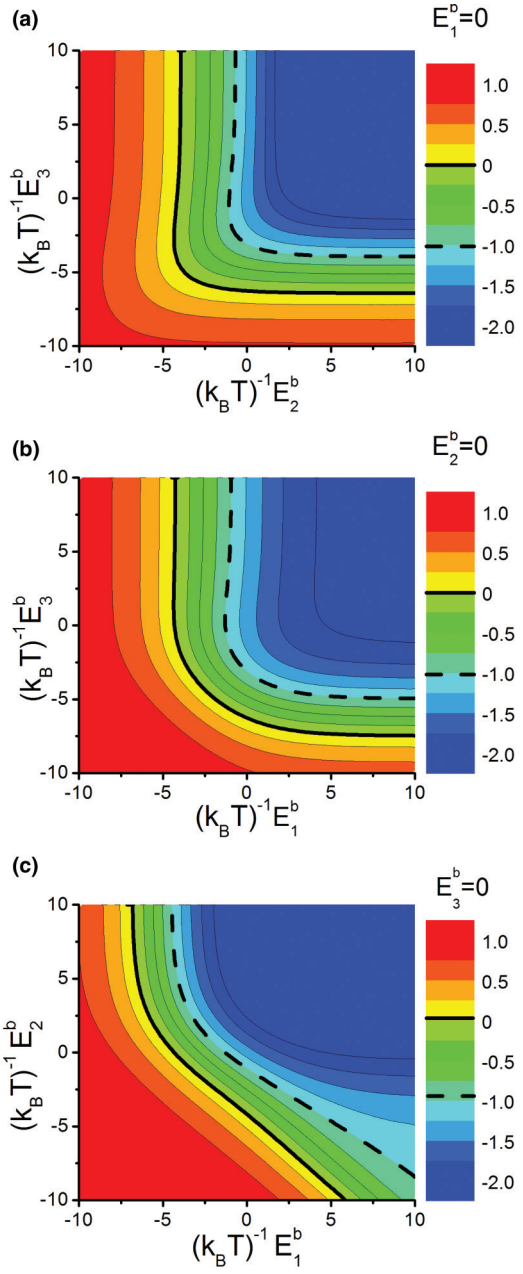

FIG. 10. (Color online) Contour map of the L_{BV}/L_{BB} ratio as a function of the interactions normalized by the inverse temperature $(k_BT)^{-1}$ in the KRA approximation. (a) for $E_1^b = 0$, (b) for $E_2^b = 0$, and (c) for $E_3^b = 0$. The black continuous line signals the onset of solute drag. The dashed line used for clarity corresponds to $L_{BV} = -L_{BB}$.

write E_1^b, E_2^b, E_3^b, with $E_d^b < 0$ for an attractive solute vacancy interaction.

We investigate a model alloy obeying the KRA approximation and for which all attempt frequencies are considered equal. This model illustrates the case of an alloy with limited kinetic effects. Calculations of the Onsager matrix by the SCMF method within the 3NN3NN approximation were performed for this alloy. Figure 10 shows the drag ratio L_{BV}/L_{BB} in this approximation as a function of the interactions normalized by the thermodynamic temperature k_BT. As expected, a strong vacancy-solute binding energy leads to solute drag. Figure 10 (bottom) demonstrates also that in a bcc alloy with a ratio $\nu^4/\nu^0 = 1$ and without second and third nearest neighbor interactions, solute drag in an alloy is still possible at low temperatures if solute-vacancy attractive interactions at a first nearest neighbor distance exceed $4k_BT$, as these interactions reduce the migration barriers for the dissociative frequency $w_{1\infty1}^{(3)}$ and increase the associative frequency $w_{11\infty}^{(4)}$. This confirms, in a more realistic case, the results from the first section according to which solute drag can take place in a bcc alloy with only first nearest neighbor solute-vacancy interaction. The KRA approximation describes the behavior of a simple model alloy, and cannot describe in all generality the kinetic behavior of alloys. It appears in good agreement with DFT calculations in some cases.[39] However, it is insufficient to accurately describe the migration barriers computed in most bcc dilute alloys such as the Fe(Cu) alloy[11,29] or the Fe(Ni) and Fe(Cr) alloys.[26,49] The interested reader is referred to Ref. 50 for a comprehensive evaluation of this approximation.

B. Broken bond model

In the parametrization of AKMC simulations for the Fe(Cu) alloy in Ref. 51 and in the line of several earlier works,[52,53] a more complex model is chosen, referred to as the broken bond (BB) model.[49,54] In this model, a species X interacts at a distance d with another species Y that can be either a vacancy or another atomic species, through pair interactions written ϵ_d^{XY} at equilibrium positions and η_d^{XY} at saddle-point positions. The energy in the initial and saddle-point configurations during an exchange between a vacancy and an atom of species A are written, respectively, $E_i = \sum_{Y,j} \epsilon_d^{vY}(j) + \sum_{Y,j} \epsilon_d^{AY}(j)$ and $E_{i,f}^S = \sum_{Y,j} \eta_d^{AY}(j)$ where the sums are performed over all the sites j.

In the dilute limit, the effect of the pair interactions ϵ_d^{Av} between the vacancy and the atoms on the equilibrium probability y_d^{Yv} and on the jump frequencies cancel each other. The Onsager matrix then depends only on the difference of interaction energies $\epsilon_d = \epsilon_d^{AB} - \epsilon_d^{AA}$ and $\eta_d = \eta_d^{AB} - \eta_d^{AA}$ for $d = 1,2,3$, and on the attempt frequencies,[55] but not on the solute vacancy interactions (cf. Appendix C). Through the saddle-point interactions, the BB model thus introduces some degrees of freedom that are absent from the KRA approximation. However, even in the absence of saddle-point interactions, the two models are not equivalent even if they show some likeness. Figure 11 shows the results of SCMF calculations for the broken bond model when the saddle-point interactions are neglected. A large domain appears where solute drag takes place.

The occurrence of drag is, however, modified by the saddle-point interactions. The 12 frequency model also allows taking into account three different ranges of saddle-point interactions. For a bcc lattice of parameter a, they correspond to saddle points at distances $\sqrt{11/16}a$, $\sqrt{19/16}a$, and $\sqrt{27/16}a$, and to exchanges between first and second nearest neighbor sites, first and third nearest neighbor sites, and to both first to fifth nearest neighbor sites and second to fourth nearest neighbor sites. Taking all of them into account introduces too many parameters for a convenient representation. However, the onset of drag can be represented at least for the simplest cases as

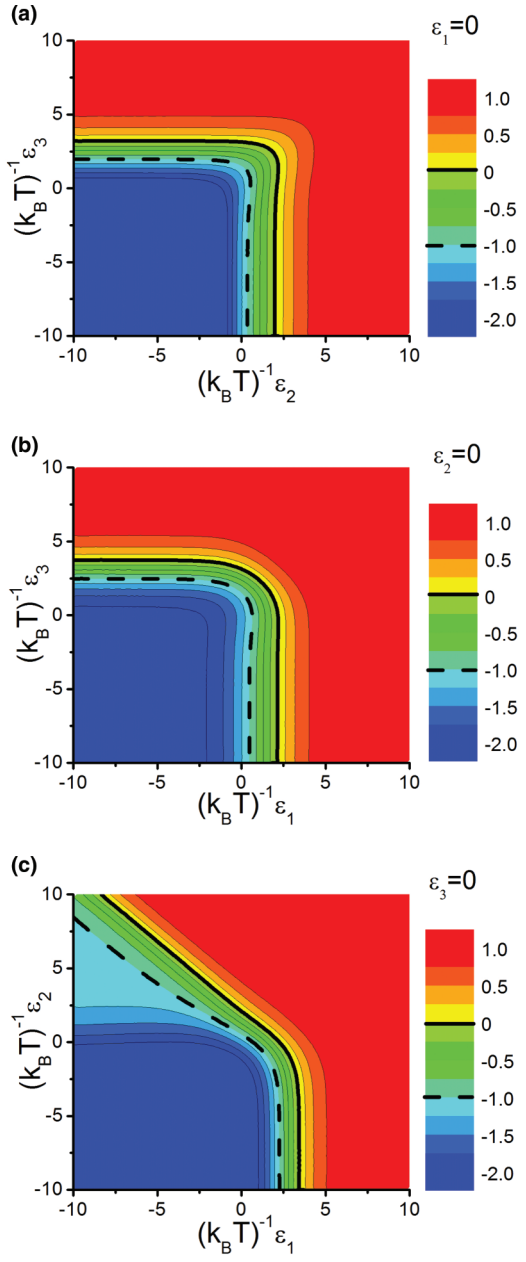

FIG. 11. (Color online) Contour map of the L_{BV}/L_{BB} ratio as a function of the interactions normalized by the inverse temperature $(k_BT)^{-1}$ in the broken bound model. (a) for $\epsilon_1 = 0$, (b) for $\epsilon_2 = 0$, (c) for $\epsilon_3 = 0$. The black continuous line signals the onset of solute drag. The dashed line, used for clarity, corresponds to $L_{BV} = -L_{BB}$.

illustrated in Fig. 12 for an alloy with interactions between first or second nearest neighbor sites at equilibrium positions and first saddle-point distances. The interaction differences ϵ_1 and ϵ_2 are represented along the horizontal and vertical axes normalized by the temperature. A given alloy can thus be represented by a line on this figure. The onset of drag, which corresponds to $L_{BV} = 0$, is represented using level lines according to the value of the ratio of the reduced first saddle-point interaction $(k_BT)^{-1}\eta_1$ by the reduced interaction energy difference $(k_BT)^{-1}\epsilon_1$. The onset of drag for a given alloy is thus obtained at the intersection between the line describing the equilibrium interactions and the level line corresponding

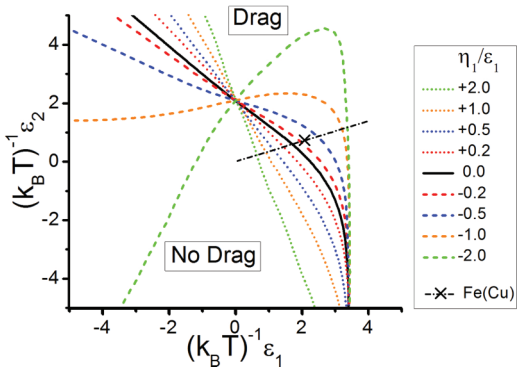

FIG. 12. (Color online) Map of the solute drag as a function of the difference of atomic interactions and for several differences of saddle-point interactions, normalized by the inverse temperature $(k_BT)^{-1}$. The × represents the temperature below which Cu atoms are dragged by the vacancies in the Fe(Cu) dilute alloy.

to the saddle-point interaction $(k_BT)^{-1}\eta$. Hence this figure provides a way to determine the qualitative behavior of an alloy without performing any additional calculations.

The first saddle-point interaction controls the 1-2 orbit, and when the saddle-point interaction increases the saddle-point energy (i.e., when $\eta > 0$), the field where the solute is dragged by the vacancies is reduced. We also note that the saddle-point interaction can even induce drag in alloys when both ϵ_1 and ϵ_2 are negative when saddle-point interactions are very low.

1. Drag effect in Fe(Cu)

Precipitation of copper in iron has attracted attention due to its possible role in the hardening and embrittlement in some reactor pressure vessel steels. From a theoretical point of view, precipitation kinetics in Fe(Cu) has been studied using various approaches (cf. Ref. 29, and references therein). First-principle calculations have been used to parametrize AKMC simulations[11,29] that produced results concerning precipitation in very good agreement with experiments. These AKMC simulations also showed solute drag effect at low temperature using solute vacancy interactions up to second nearest neighbor sites. These simulations are characterized by a strong vacancy-copper binding energy on first and second nearest neighbor sites.

In Ref. 29, with second nearest neighbor interactions, eight different frequencies are required to describe diffusion, and the Onsager matrix could not be analytically obtained using the methods previously available.[32,33] Figure 12 allows immediate identification of the qualitative behavior of this alloy. The dash-dotted line represents the equation $\beta\epsilon_2 = 0.346\beta\epsilon_1 - 0.041$ which describes the equilibrium properties of the Fe(Cu) dilute alloy. The value of the saddle-point interaction $\beta\eta = -0.24\beta\epsilon_1 + 0.0027$ provides then the point at which drag starts, for $\beta\epsilon_1 \approx 2.1$, i.e., $T \approx 700$ K.

The quantitative behavior can be obtained by performing SCMF calculations in the 3NN3NN approximation for the Fe(Cu) alloy. In Fig. 13, the ratio L_{BV}/L_{BB} obtained by Soisson *et al.*[56] using AKMC simulations is plotted as a function of temperature, and compared with calculations in the 3NN3NN approximation using the same jump frequencies. A remarkable agreement is obtained on the whole temperature

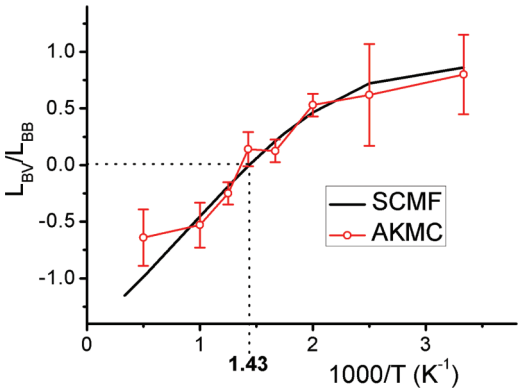

FIG. 13. (Color online) Drag ratio L_{BV}/L_{BB} as a function of the temperature in a dilute Fe(Cu) alloy described by the 12 frequency model. This alloy is described by a broken bond model using the interactions $\epsilon_1 = 0.127 - 7.83 \times 10^{-6}T$ eV, $\epsilon_2 = 0.044 - 3.92 \times 10^{-6}T$ eV, and $\eta_1 = 0.17$ eV (Ref. 56). Open circles represent the results of AKMC simulations from Ref. 56, while the continuous line represents 3NN3NN SCMF calculations.

range explored, with the copper atoms being dragged by the vacancies below 700 K.

VI. CONCLUSION

The goal of this study was to identify cases where solute drag by vacancies could take place in bcc alloys. To that end, calculations of the Onsager matrix in dilute bcc alloys have been performed using an analytic method. The SCMF method has been extended for that purpose, to account for solute-vacancy interactions at a distance up to third nearest neighbor and increased kinetic correlations in bcc alloys. One of the first results of this paper is the derivation of analytic expressions for the Onsager coefficients in this case.

The extension of the SCMF method makes it possible to analytically calculate the Onsager matrix of ideal solutions which is used here to study the mechanisms responsible for solute drag. Several paths were identified for the vacancy to orbit around the solute atoms. Collective effects, involving different types of jumps, showed that low escape frequencies could also trigger solute drag if they were able to create an orbit around a solute. Finally, calculations applied to a typical alloy with interactions up to third nearest neighbor sites were performed to help identifying cases where solute drag could take place. SCMF results proved that solute drag occurs under a broader set of conditions than predicted by previous calculations.

It is well accepted that for solute drag to take place, a vacancy should be able to orbit around a solute atom while interacting with the impurity during several successive jumps. This study shows, however, that these orbits should be defined from a *kinetic* point of view, and controlled by the jump frequencies and not by the range of the solute-vacancy binding energy. In a bcc alloy where the solute-vacancy binding energy is limited to first nearest neighbor sites and if the impurity does not affect jump rates toward these first nearest neighbor sites ($w^{(4)} = w^{(0)}$) no solute drag occurs. However, solute drag may occur when jumps toward these sites are affected by the impurity. It should be noticed that this is the case when using approximations such as the KRA approximation or the broken bond model with only first nearest neighbor interactions, where the saddle point of jumps leading toward the first nearest neighbors is also affected by the presence of an impurity. As a consequence traditional analytic calculations in the first shell approximation are insufficient as they fail to capture qualitative aspects of solute drag in many cases. More accurate mean field calculations like the one performed in the 3NN3NN approximation, however, overcome these limitations. AKMC simulations were used to confirm this prediction as well as to assess the ability of SCMF calculations to quantitatively provide the Onsager matrix for model alloys and for the model of a Fe(Cu) alloy studied in Ref. 29. The SCMF is a promising general method for the computation of Onsager coefficients. The present method can be extended to arbitrary crystal structures, to compute the kinetic properties of alloys.

ACKNOWLEDGMENTS

The authors thank J. L. Bocquet for his involvement and interest in the method. F. Soisson is thanked for fruitful discussions on the Fe(Cu) alloy, L. Messina for the exchanges on the SCMF method, and J. Tucker for providing extra information on her methodology. This research is partly supported by the DOE-BES Grant No. DE-FG02-05ER46217, and by the DOE-BES Computational Materials and Chemical Sciences Network on "Computational Microstructure Science."

APPENDIX A: ANALYTIC EXPRESSIONS FOR 3NN3NN SCMF COMPUTATIONS IN bcc ALLOYS

We provide the analytic elements required to obtain the Onsager matrix in the 3NN3NN approximation for a bcc dilute alloy. All this elements are available in a symbolic form in the Supplemental Materials with a routine that compute the Onsager matrix from a set of twelve frequencies.[57] The notations of Sec. II B are used. For a binary alloy, only the effective interactions associated to the pair of species *A*-*B* needs to be considered. As a consequence, T is a C by C matrix where C is the number of symmetry classes considered. A vector belonging to each of the symmetry classes can be used to represent them. These vectors are provided in Table I and Fig. 14 shows these vectors on a bcc lattice. The indices of the symmetry classes in Table I and Fig. 14 correspond also to the order in which they are being used in the following symbolic expressions. Additionally, we use the

TABLE I. Cartesian coordinates of a representive of each of the bond classes, for diffusion in the (100) direction. The indices in this table are identical to the row or column numbers used in the symbolic quantities expressions.

Index	Vector	Index	Vector
1	$\frac{a}{2}[111]$	8	$\frac{a}{2}[133]$
2	$a[100]$	9	$\frac{a}{2}[331]$
3	$a[110]$	10	$a[120]$
4	$\frac{a}{2}[131]$	11	$a[210]$
5	$\frac{a}{2}[311]$	12	$a[121]$
6	$a[111]$	13	$a[211]$
7	$a[200]$	14	$a[221]$

notation $T = R + \mathrm{Diag}(D)$.

$$R = \begin{pmatrix}
0 & -W_{121}^{(1)} & -2W_{131}^{(1)} & 0 & 0 & -W_{1\infty1}^{(3)} & 0 & 0 & 0 & 0 & 0 & 0 & 0 & 0 \\
-4W_{112}^{(1)} & 0 & 0 & 0 & -4W_{1\infty2}^{(3)} & 0 & 0 & 0 & 0 & 0 & 0 & 0 & 0 & 0 \\
-2W_{113}^{(1)} & 0 & 0 & -2W_{1\infty3}^{(3)} & -2W_{1\infty3}^{(3)} & 0 & 0 & 0 & -2W_{1\infty3}^{(3)} & 0 & 0 & 0 & 0 & 0 \\
0 & 0 & -W_{13\infty}^{(4)} & 0 & 0 & -W_1^{(0)} & 0 & 0 & 0 & -W_1^{(0)} & 0 & -W_1^{(0)} & 0 & 0 \\
0 & -W_{12\infty}^{(4)} & -2W_{13\infty}^{(4)} & 0 & 0 & -W_1^{(0)} & -W_1^{(0)} & 0 & 0 & 0 & -2W_1^{(0)} & 0 & -W_1^{(0)} & 0 \\
-W_{11\infty}^{(4)} & 0 & 0 & -2W_1^{(0)} & -W_1^{(0)} & & 0 & -W_1^{(0)} & -2W_1^{(0)} & 0 & 0 & 0 & 0 & 0 \\
0 & 0 & 0 & 0 & -4W_1^{(0)} & 0 & 0 & 0 & 0 & 0 & 0 & 0 & 0 & 0 \\
0 & 0 & 0 & 0 & 0 & -W_1^{(0)} & 0 & 0 & 0 & 0 & 0 & -2W_1^{(0)} & 0 & 0 \\
0 & 0 & -W_{13\infty}^{(4)} & 0 & 0 & -W_1^{(0)} & 0 & 0 & 0 & -W_1^{(0)} & -W_1^{(0)} & -W_1^{(0)} & -W_1^{(0)} & -W_1^{(0)} \\
0 & 0 & 0 & -2W_1^{(0)} & 0 & 0 & 0 & 0 & -2W_1^{(0)} & 0 & 0 & 0 & 0 & 0 \\
0 & 0 & 0 & 0 & -2W_1^{(0)} & 0 & 0 & 0 & -2W_1^{(0)} & 0 & 0 & 0 & 0 & 0 \\
0 & 0 & 0 & -W_1^{(0)} & 0 & 0 & 0 & -W_1^{(0)} & -W_1^{(0)} & 0 & 0 & 0 & 0 & 0 \\
0 & 0 & 0 & 0 & -W_1^{(0)} & 0 & 0 & 0 & -2W_1^{(0)} & 0 & 0 & 0 & 0 & 0 \\
0 & 0 & 0 & 0 & 0 & 0 & 0 & 0 & -2W_1^{(0)} & 0 & 0 & 0 & 0 & 0
\end{pmatrix}, \tag{A1}$$

$$D = \begin{pmatrix}
3W_{121}^{(1)} + 3W_{131}^{(1)} + 2W_1^{(2)} + W_{1\infty1}^{(3)} \\
4W_{112}^{(1)} + 4W_{1\infty2}^{(3)} \\
2W_{113}^{(1)} + 6W_{1\infty3}^{(3)} \\
5W_1^{(0)} + W_{12\infty}^{(3)} + 2W_{13\infty}^{(3)} \\
5W_1^{(0)} + W_{12\infty}^{(3)} + 2W_{13\infty}^{(3)} \\
7W_1^{(0)} + W_{11\infty}^{(3)} \\
8W_1^{(0)} \\
7W_1^{(0)} + W_{13\infty}^{(3)} \\
7W_1^{(0)} + W_{13\infty}^{(3)} \\
8W_1^{(0)} \\
8W_1^{(0)} \\
8W_1^{(0)} \\
8W_1^{(0)} \\
8W_1^{(0)}
\end{pmatrix}, \tag{A2}$$

$$(\vec{M}^{AB,A}) \cdot \vec{u} = \frac{a}{2} \begin{pmatrix}
W_{121}^{(1)} - W_{131}^{(1)} - W_{1\infty1}^{(3)} \\
4W_{112}^{(1)} - 4W_{1\infty2}^{(3)} \\
2W_{113}^{(1)} - 2W_{1\infty3}^{(3)} \\
W_{12\infty}^{(4)} - W_1^{(0)} \\
W_{12\infty}^{(4)} - 3W_1^{(0)} + 2W_{13\infty}^{(4)} \\
W_{11\infty}^{(4)} - W_1^{(0)} \\
0 \\
W_{13\infty}^{(4)} - W_1^{(0)} \\
W_{13\infty}^{(4)} - W_1^{(0)} \\
0 \\
0 \\
0 \\
0 \\
0
\end{pmatrix}, \tag{A3}$$

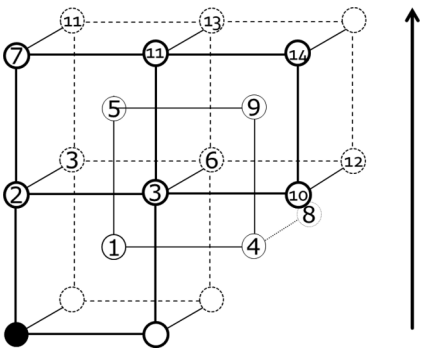

FIG. 14. Schematic representation of the classes of bonds associated to the different rows and columns of the T matrix. The number on an atomic site is the class represented by the vector linking the black site to this site. The arrow represents the direction of diffusion.

$$(\vec{M}^{AB,B}) \cdot \vec{u} = \frac{a}{2} \begin{pmatrix}
-W_1^{(2)}/2 \\
0 \\
0 \\
0 \\
0 \\
0 \\
0 \\
0 \\
0 \\
0 \\
0 \\
0 \\
0 \\
0
\end{pmatrix}, \tag{A4}$$

$$(\Lambda^{A,AB}) = \begin{pmatrix} W^{(1)}_{131} - W^{(1)}_{121} + W^{(3)}_{1\infty1} \\ W^{(3)}_{1\infty2} - W^{(1)}_{112} \\ 2W^{(3)}_{1\infty3} - 2W^{(1)}_{113} \\ 2W^{(0)}_{1} - 2W^{(4)}_{12\infty} \\ 3W^{(0)}_{1} - W^{(4)}_{12\infty} - 2W^{(4)}_{13\infty} \\ W^{(0)}_{1} - W^{(4)}_{11\infty} \\ 0 \\ W^{(0)}_{1} - W^{(4)}_{13\infty} \\ 2W^{(0)}_{1} - 2W^{(4)}_{13\infty} \\ 0 \\ 0 \\ 0 \\ 0 \\ 0 \end{pmatrix}, \tag{A5}$$

$$(\Lambda^{B,AB}) = \begin{pmatrix} W^{(2)}_{1} \\ 0 \\ 0 \\ 0 \\ 0 \\ 0 \\ 0 \\ 0 \\ 0 \\ 0 \\ 0 \\ 0 \\ 0 \\ 0 \end{pmatrix}. \tag{A6}$$

As jumps are limited to nearest neighbor sites only, there is a single class of nonzero contribution to the bare mobility

$$\begin{aligned} l^{AA}_{(0)} &= \mathfrak{X}^{(0)}_1 + 3\mathfrak{X}^{(1)}_{112} + 3\mathfrak{X}^{(1)}_{121} + 3\mathfrak{X}^{(1)}_{113} + 3\mathfrak{X}^{(1)}_{131} + \mathfrak{X}^{(3)}_{1\infty1} \\ &\quad + 3\mathfrak{X}^{(3)}_{1\infty2} + 9\mathfrak{X}^{(3)}_{1\infty3} + \mathfrak{X}^{(4)}_{11\infty} + 3\mathfrak{X}^{(4)}_{12\infty} + 9\mathfrak{X}^{(4)}_{13\infty}, \\ l^{BB}_{(0)} &= \mathfrak{X}^{(2)}_1. \end{aligned} \tag{A7}$$

To each thermodynamic average can be substituted the expression in terms of the concentration in vacancy solute and binding energies:

$$\begin{aligned} W^{(0)}_1 &= c_v c_B w^{(0)}_1, \\ W^{(2)}_1 &= c_v c_B y^{B\nu}_1 w^{(2)}_1, \\ W^{(1)}_{112} &= c_v c_B y^{B\nu}_1 w^{(2)}_{112}, \\ W^{(1)}_{121} &= c_v c_B y^{B\nu}_1 w^{(1)}_{121}, \\ W^{(1)}_{113} &= c_v c_B y^{B\nu}_3 w^{(1)}_{113}, \\ W^{(1)}_{131} &= c_v c_B y^{B\nu}_1 w^{(1)}_{131}, \\ W^{(3)}_{141} &= c_v c_B y^{B\nu}_1 w^{(3)}_{141}, \\ W^{(3)}_{142} &= c_v c_B y^{B\nu}_2 w^{(3)}_{142}, \\ W^{(3)}_{143} &= c_v c_B y^{B\nu}_3 w^{(3)}_{143}, \\ W^{(4)}_{114} &= c_v c_B w^{(4)}_{114}, \\ W^{(4)}_{124} &= c_v c_B w^{(4)}_{124}, \\ W^{(4)}_{134} &= c_v c_B w^{(4)}_{134}, \end{aligned} \tag{A8}$$

$$\begin{aligned} \mathfrak{X}^{(0)}_1 &= c_v w^{(0)}_1 \big[1 - c_b \big(8y^{B\nu}_1 + 6y^{B\nu}_2 + 12y^{B\nu}_3 + 13\big)\big], \\ \mathfrak{X}^{(2)}_1 &= c_v c_B y^{B\nu}_1 w^{(2)}_1, \\ \mathfrak{X}^{(1)}_{112} &= c_v c_B y^{B\nu}_2 w^{(1)}_{112}, \\ \mathfrak{X}^{(1)}_{121} &= c_v c_B y^{B\nu}_1 w^{(1)}_{121}, \\ \mathfrak{X}^{(1)}_{113} &= c_v c_B y^{B\nu}_3 w^{(1)}_{113}, \\ \mathfrak{X}^{(1)}_{131} &= c_v c_B y^{B\nu}_1 w^{(1)}_{131}, \\ \mathfrak{X}^{(3)}_{141} &= c_v c_B y^{B\nu}_1 w^{(3)}_{141}, \\ \mathfrak{X}^{(3)}_{142} &= c_v c_B y^{B\nu}_2 w^{(3)}_{142}, \\ \mathfrak{X}^{(3)}_{143} &= c_v c_B y^{B\nu}_3 w^{(3)}_{143}, \\ \mathfrak{X}^{(4)}_{114} &= c_v c_B w^{(4)}_{114}, \\ \mathfrak{X}^{(4)}_{124} &= c_v c_B w^{(4)}_{124}, \\ \mathfrak{X}^{(4)}_{134} &= c_v c_B w^{(4)}_{134}. \end{aligned} \tag{A9}$$

As an example, considering explicitly the thermodynamic prefactors for the bare mobility leads to the expressions:

$$\begin{aligned} l^{AA}_{(0)} &= c_\nu \big[1 - c_B \big(13 + 8y^{B\nu}_1 + 6y^{B\nu}_2 + 12y^{B\nu}_3\big)\big] w^{(0)}_1 \\ &\quad + 6c_\nu c_B y^{B\nu}_2 w^{(1)}_{112} + 6c_\nu c_B y^{B\nu}_3 w^{(1)}_{113} \\ &\quad + 2c_\nu c_B w^{(4)}_{11\infty} + 6c_\nu c_B w^{(4)}_{12\infty} + 18c_\nu c_B w^{(4)}_{13\infty}, \\ l^{BB}_{(0)} &= c_\nu c_B y^{B\nu}_1 w^{(2)}_1. \end{aligned} \tag{A10}$$

APPENDIX B: AKMC SIMULATIONS

Atomic kinetic Monte Carlo simulation is a standard method to describe the evolution of the microstructure of alloys. A state of the alloy is defined by a vector $\mathbf{n}$, the components of which are the occupation numbers of all species on all sites of a rigid lattice $\{n^A_1, n^B_1, \ldots, n^\nu_1; n^A_2, n^B_2, \ldots, n^\nu_2; \ldots\}$ such that $n^X_i = 1$ if the site i is occupied by the species $X \in \{\nu, A, B \ldots\}$ and zero otherwise. It is assumed that the different species diffuse from lattice site to lattice site without the lattice itself being affected. The evolution is controlled by an algorithm like the residence time algorithm introduced by Young *et al.*[58] At each iteration the following operations are performed:

(1) Updating the list $\{\dot{\mathbf{n}}\}$ of possible configurations connected to the current configuration by a single step.

(2) Computing the transition rates $W(\mathbf{n} \to \dot{\mathbf{n}})$ of each transition.

(3) Selecting a pseudorandom number R of uniform probability over [0,1).

(4) Choosing the event i for which
$\sum^{i-1}_{\mathbf{n}_j \in \{\dot{\mathbf{n}}\}} W(\mathbf{n} \to \mathbf{n}_j) \leqslant R < \sum^{i}_{\mathbf{n}_j \in \{\dot{\mathbf{n}}\}} W(\mathbf{n} \to \mathbf{n}_j)$.

(5) Increasing the physical time of the simulation by the inverse of the sum of the transition rates $\Delta t = \frac{1}{\sum_{\dot{\mathbf{n}}} W(\mathbf{n} \to \dot{\mathbf{n}})}$.

(6) Updating $\mathbf{n}$ to the new state.

In the case of a vacancy-mediated diffusion process, the list of the transitions contains all possible vacancy-atom exchanges. In the case of a bcc alloy, only first nearest neighbor exchanges are considered.

In order to compute the Onsager matrix in the dilute limit, a single vacancy and a single solute atom B are randomly introduced in a simulation box filled with atoms A, with periodic boundary conditions. The system is then equilibrated to ensure that the solute-vacancy distance obeys a Boltzmann distribution. The displacements of atoms are then registered after each step of the residence time algorithm to integrate the displacement of all species. For the simulations performed in the current work, a simulation box of 2×16^3 atomic sites has been used, and the integration has been performed over 100 MCS and averaged over 10^5 samples to obtain the thermodynamic average. The vacancy and solute concentrations are larger in AKMC simulations than in real dilute systems. The time can be renormalized to take this fact into account.[59] However, in the present case the terms of the Onsager matrix are linear with respect to the concentration in vacancy and solutes. As a consequence, the drag ratio L_{BV}/L_{BB} is independent of both concentrations.

APPENDIX C: INTERACTIONS IN THE BROKEN BOND MODEL

The total probability to find a transition from an initial configuration i to a final configuration f can be written as

$$P_{\text{tot}} = P(i) w_{i\to f}, \tag{C1}$$

where the probability $P(i)$ to find the system in the configuration i can be written in the dilute limit using the binding energy E_i^b as $P(i) = \frac{e^{-(k_B T)^{-1} E_i^b}}{\mathfrak{Z}}$, where $\mathfrak{Z}$ is the partition function, and the transition probability $w_{i\to f}$ as $w_{i\to f} = \nu e^{-(k_B T)^{-1}(E_{i,f}^S - E_i)}$, with E_i the energy in the initial configuration and $E_{i,f}^S$ the saddle-point energy. In the dilute limit the binding energy E_i^b in a configuration i is the difference between the energy E^c of the system in the configuration i where the solute and the vacancy are at a finite distance c and the energy of a system where solute and vacancies are at infinite distance E_∞:

$$E_i^b = E^c - E_\infty. \tag{C2}$$

In the BB model, they can be written as

$$\begin{aligned} E_\infty &= E^0 + \sum_x Z_x \epsilon_x^{BA} + Z_x \epsilon_x^{AV}, \\ E^c &= E^0 - \epsilon_c^{AB} + \epsilon_c^{BV} - \epsilon_c^{AV} + \epsilon_c^{AA} \\ &\quad + \sum_x Z_x \epsilon_x^{BA} + Z_x \epsilon_x^{AV}, \end{aligned} \tag{C3}$$

where the sums are performed over all distances x between the solute and the vacancy, Z_x is the number of neighboring sites at a distance x, V is a vacancy, A is a matrix atom, and B is a solute atom. The binding energy can finally be written as

$$E_i^b = \left(\epsilon_c^{BV} - \epsilon_c^{AV}\right) - \left(\epsilon_c^{AB} - \epsilon_c^{AA}\right). \tag{C4}$$

The migration energy associated to a frequency $w_{abc}^{(\zeta)}$ *as computed in the BB model*, corresponds to the following difference of local energies:

$$\begin{aligned} E_{i,f}^{\text{mig}} = E_{i,f}^S - \Bigg(&\sum_x Z_x \epsilon_x^{AA} + \sum_x Z_x \epsilon_x^{AV} \\ &+ \left(\epsilon_c^{BV} - \epsilon_c^{AV}\right) + \left(\epsilon_b^{AB} - \epsilon_b^{AA}\right) \Bigg), \end{aligned} \tag{C5}$$

where b is the distance between the jumping atom and the solute in the initial configuration and c is the distance between the vacancy and the solute, as defined in the nomenclature section. As a consequence, from Eqs. (C1), (C4), and (C5) the total migration probability can be written as

$$P_{\text{tot}} = \mathfrak{A} \exp\left\{+(k_B T)^{-1}\left[\left(\epsilon_c^{AB} - \epsilon_c^{AA}\right) + \left(\epsilon_b^{AB} - \epsilon_b^{AA}\right)\right]\right\}, \tag{C6}$$

with $\mathfrak{A} = \mathfrak{Z}^{-1} \exp\{-(k_B T)^{-1}[E_{i,f}^S - (\sum_x Z_x \epsilon_x^{AA} + \sum_x Z_x \epsilon_x^{AV})]\}$. As a consequence, the drag ratio L_{BV}/L_{BB} depends only on the differences of interactions $\epsilon_k = \epsilon_k^{AB} - \epsilon_k^{AA}$ and on the saddle-point interactions difference $\eta_k = \eta_k^{AB} - \eta_k^{AA}$.

*tgarnier@illinois.edu

[1] V. I. Yelagin, V. V. Zakharov, S. G. Pavlenko, and T. D. Rostova, Phys. Met. Metallogr. **60**, 88 (1986).

[2] E. Clouet, L. Laé, T. Épicier, W. Lefebvre, M. Nastar, and A. Deschamps, Nat. Mater. **5**, 482 (2006).

[3] F. Danoix, E. Bemont, P. Maugis, and D. Blavette, Adv Eng. Mater. **8**, 1202 (2006).

[4] Z. Mao, C. K. Sudbrack, K. E. Yoon, G. Martin, and D. N. Seidman, Nat. Mater. **6**, 210 (2007).

[5] A. Barbu and G. Martin, Scr. Metall. **11**, 771 (1977).

[6] A. Barbu, G. Martin, and A. Chamberod, J. Appl. Phys. **51**, 6192 (1980).

[7] M. Nastar and F. Soisson, *Comprehensive Nuclear Materials* (Elsevier, New York, 2012), Chap. 1.18, pp. 471–496.

[8] Z. Jiao and G. Was, Acta Mater. **59**, 1220 (2011).

[9] M. Nastar, Philos. Mag. A **85**, 641 (2005).

[10] A. Ardell, *Materials Issues for Generation IV Systems* (Springer, New York, 2008), pp. 285–310.

[11] A. V. Barashev and A. C. Arokiam, Philos. Mag. Lett. **86**, 321 (2006).

[12] A. Barbu and A. J. Ardell, Scr. Metall. **9**, 1233 (1975).

[13] H. Wan, Y. Shen, X. Jin, Y. Chen, and J. Sun, Acta Mater. **60**, 2528 (2012).

[14] P. Bellon, *Comprehensive Nuclear Materials* (Elsevier, New York, 2012), Chap. 1.15, pp. 411–432.

[15] J. Ågren, Metall. Mater. Trans. A **43**, 3453 (2011).

[16] T. Anthony, J. Appl. Phys. **41**, 3969 (1970).

[17] T. Anthony, *Proceeding of Conference Atomic Transport in Solids and Liquids, Marstransd, 1970* (Verlag der Zeitschrift für Naturforschung, Tübingen, 1971), p. 138.

[18] T. Anthony, *Proceeding of Conference Radiation-Induced Voids in Metals, Albany* (US atomic energy commission, State University of New York, Albany, 1972), p. 630.

[19]T. Anthony, Acta Metall. **17**, 603 (1969).
[20]M. Jones and A. Le Claire, Philos. Mag. **26**, 1191 (1972).
[21]A. Van der Ven and G. Ceder, Phys. Rev. Lett. **94**, 045901 (2005).
[22]M. Mantina, Y. Wang, R. Arroyave, L. Q. Chen, Z. K. Liu, and C. Wolverton, Phys. Rev. Lett. **100**, 215901 (2008).
[23]M. Mantina, Y. Wang, L. Chen, Z. Liu, and C. Wolverton, Acta Mater. **57**, 4102 (2009).
[24]J. Tucker, R. Najafabadi, T. Allen, and D. Morgan, J. Nucl. Mater. **405**, 216 (2010).
[25]S. Choudhury, L. Barnard, J. Tucker, T. Allen, B. Wirth, M. Asta, and D. Morgan, J. Nucl. Mater. **411**, 1 (2011).
[26]L. Barnard, J. Tucker, S. Choudhury, T. Allen, and D. Morgan, J. Nucl. Mater. **425**, 8 (2012).
[27]L. Messina, Z. Chang, and P. Olsson, Nucl. Instrum. Methods Phys. Res., Sect. B. **01**, 049 (2013).
[28]A. C. Arokiam, A. V. Barashev, D. J. Bacon, and Y. N. Osetsky, Phys. Rev. B **71**, 174205 (2005).
[29]F. Soisson and C. C. Fu, Phys. Rev. B **76**, 214102 (2007).
[30]A. R. Allnatt and A. B. Lidiard, *Atomic Transport in Solids* (Cambridge University Press, Cambridge, 1993).
[31]A. Barbu and A. Lidiard, Philos. Mag. A **74**, 709 (1996).
[32]Y. Serruys and G. Brebec, Philos. Mag. A **46**, 661 (1982).
[33]Y. Okamura and A. R. Allnatt, J. Phys. C **16**, 1841 (1983).
[34]M. Nastar, V. Y. Dobretsov, and G. Martin, Philos. Mag. **80**, 155 (2000).
[35]M. Nastar, Philos. Mag. **85**, 3767 (2005).
[36]T. Anthony, *Diffusion in Solids: Recent Developments* (Academic, New York, 1975), Chap. 7, pp. 353–378.
[37]J. M. Sanchez, F. Ducastelle, and D. Gratias, Physica A **128**, 334 (1984).
[38]J. Philibert, *Atom Movements: Diffusion and Mass Transport in Solids* (Editions de Physique, Les Ulis, France, 1991).
[39]T. Garnier, V. R. Manga, D. R. Trinkle, M. Nastar, and P. Bellon, Phys. Rev. Lett. (unpublished).
[40]T. Garnier, D. Trinkle, P. Bellon, and M. Nastar (unpublished).
[41]E. Clouet and M. Nastar, Phys. Rev. B **75**, 132102 (2007).
[42]A. C. Arokiam, A. V. Barashev, D. J. Bacon, and Y. N. Osetsky, Philos. Mag. **87**, 925 (2007).
[43]N. V. Doan and J.-L. Bocquet, Thin Solid Films **25**, 15 (1975).
[44]A. R. Allnatt and E. Allnatt, Philos. Mag. A **64**, 341 (1991).
[45]J. Manning, Phys. Rev. **136**, A1758 (1964).
[46]A. Senhaji, G. Treglia, B. Legrand, N. Barrett, C. Guillot, and B. Villette, Surf. Sci. **274**, 297 (1992).
[47]A. Van der Ven, G. Ceder, M. Asta, and P. D. Tepesch, Phys. Rev. B **64**, 184307 (2001).
[48]E. Vincent, C. S. Becquart, and C. Domain, Nucl. Instrum. Methods Phys. Res. B **255**, 78 (2006).
[49]E. Martinez, O. Senninger, C.-C. Fu, and F. Soisson, Phys. Rev. B **86**, 224109 (2012).
[50]J. L. Bocquet, Defect Diffus. Forum **203–205**, 81 (2002).
[51]F. Soisson, J. Nucl. Mater. **349**, 235 (2006).
[52]E. Salomons, P. Bellon, F. Soisson, and G. Martin, Phys. Rev. B **45**, 4582 (1992).
[53]F. Soisson, P. Bellon, and G. Martin, Phys. Rev. B **46**, 11332 (1992).
[54]F. Soisson and G. Martin, Phys. Rev. B **62**, 203 (2000).
[55]Entropic contribution usually included in the attempt frequency can also be introduced in the interaction energy difference using a temperature-dependent migration enthalpy.
[56]F. Soisson and C.-C. Fu, Solid State Phenom. **139**, 107 (2008).
[57]See Supplemental Material at http://link.aps.org/supplemental/10.1103/PhysRevB.88.134201.
[58]W. Young and E. Elcock, Proc. Phys. Soc. **89**, 735 (1966).
[59]M. Nastar and F. Soisson, Phys. Rev. B **86**, 220102 (2012).